Generation of Leaf Shape Through Early Patterns of Growth and Tissue Polarity

Erika E. Kuchen, *et al.*

Science **335**, 1092 (2012);
DOI: 10.1126/science.1214678

By measuring reinforcing selection acting on the dark flower–color allele in *P. drummondii* under natural sympatric conditions and by quantifying selection in the absence of *P. cuspidata*, we were able to compare the relative strengths of direct selection by other environmental factors and by reinforcing selection on a trait conferring increased premating isolation in a region of sympatry. The absence of detectable fitness differences among flower color genotypes in the absence of *P. cuspidata* indicates that another agent of selection is unlikely to be involved in flower color divergence in *P. drummondii*. Although we cannot rule out small, statistically undetectable differences in survival or reproductive success favoring these genotypes, such differences would be of minor importance compared with the strong reinforcing selection acting on the intensity locus.

Many plants have evolved premating reproductive isolation by switching pollinator types (e.g., from bees to hummingbirds) (*22*–*24*). Our work suggests that increased reproductive isolation can also be achieved by a single pollinator species through constancy of individual pollinators. In particular, if pollinators transition between flowers with similar phenotypes more frequently then between flowers with unlike phenotypes, this will decrease gene flow between unlike flowers. Constancy is commonly studied in bumble bees but rarely investigated in butterfly pollinators (*20*, *25*). That the primary pollinator *Battus philenor* exhibits this type of constancy is not surprising, given that females of this species exhibit constancy for leaf shape when searching for oviposition sites (*21*).

Theoretical models indicate that the likelihood of successful reinforcement is greater when selection is strong, because this will counteract gene flow and recombination, which tend to reduce premating isolation (*26*–*28*). Our results indicate that, at least in some cases, very strong reinforcing selection may act on a single allele and lead to increased reproductive isolation.

Theory also indicates that reinforcement is more easily achieved by a one-allele mechanism (*4*, *29*), but empirical assessment of this prediction has been difficult because the genetic basis of reinforcement is understood in few systems (*7*). Our current demonstration of reinforcing selection acting on the dark allele indicates that reinforcement in *P. drummondii* involves a two-allele reinforcement mechanism. The intensity locus causes reproductive isolation only if the dark allele is present in *P. drummondii* and the light allele is present in *P. cuspidata*. Consistent with theory, we find that strong selection and high levels of hybrid sterility cause the spread of the dark allele through sympatric *P. drummondii* populations. We suspect all reinforcement mechanisms involving different floral phenotypes to which pollination vectors must respond will be two-allele assortative mating mechanisms, because pollinators must be able to discriminate between the novel phenotype in one species and the ancestral phenotype in both species.

Although reinforcement has been studied primarily in animals (*3*, *7*), our work indicates that it may also be an important contributor to speciation in plants. If so, this phenomenon may provide a partial explanation for the tremendous diversity of floral color, floral morphology, and inflorescence structure that characterize flowering plants.

References and Notes

1. R. Butlin, *Trends Ecol. Evol.* **2**, 8 (1987).
2. T. Dobzhansky, *Genetics and the Origin of Species* (Columbia Univ. Press, New York, 1937).
3. D. J. Howard, in *Hybrid Zones and the Evolutionary Process*, R. G. Harrison, Ed. (Oxford Univ. Press, New York, 1993), pp. 46–69.
4. M. R. Servedio, M. A. F. Noor, *Annu. Rev. Ecol. Evol. Syst.* **34**, 339 (2003).
5. A. R. Wallace, *Darwinism: An Exposition of the Theory of Natural Selection, with Some of Its Applications* (Macmillan, London, 1889).
6. M. Kirkpatrick, V. Ravigné, *Am. Nat.* **159** (suppl. 3), S22 (2002).
7. D. Ortiz-Barrientos, A. Grealy, P. Nosil, *Ann. N. Y. Acad. Sci.* **1168**, 156 (2009).
8. M. Kirkpatrick, *Proc. R. Soc. London Ser. B* **267**, 1649 (2000).
9. M. Kirkpatrick, M. R. Servedio, *Genetics* **151**, 865 (1999).
10. M. R. Servedio, *Evolution* **55**, 1909 (2001).
11. M. R. Servedio, *Evolution* **58**, 913 (2004).
12. A. Y. K. Albert, D. Schluter, *Evolution* **58**, 1099 (2004).
13. P. Nosil, B. J. Crespi, C. P. Sandoval, *Proc. R. Soc. London Ser. B* **270**, 1911 (2003).
14. D. A. Levin, *Evolution* **39**, 1275 (1985).
15. R. Hopkins, D. A. Levin, M. D. Rausher, *Evolution* **66**, 469 (2012).
16. D. A. Levin, *Am. J. Bot.* **54**, 1122 (1967).
17. L. G. Ruane, K. Donohue, *Evol. Ecol.* **22**, 229 (2008).
18. R. Hopkins, M. D. Rausher, *Nature* **469**, 411 (2011).
19. Material and methods are available as supporting material on *Science* Online.
20. N. M. Waser, *Am. Nat.* **127**, 593 (1986).
21. M. D. Rausher, *Science* **200**, 1071 (1978).
22. H. D. Bradshaw Jr., D. W. Schemske, *Nature* **426**, 176 (2003).
23. D. R. Campbell, N. M. Waser, E. J. Melendez-Ackerman, *Am. Nat.* **149**, 295 (1997).
24. M. E. Hoballah *et al.*, *Plant Cell* **19**, 779 (2007).
25. L. Chittka, J. D. Thomson, N. M. Waser, *Naturwissenschaften* **86**, 361 (1999).
26. M. Caisse, J. Antonovics, *Heredity* **40**, 371 (1978).
27. J. Felsenstein, *Evolution* **35**, 124 (1981).
28. L. W. Liou, T. D. Price, *Evolution* **48**, 1451 (1994).
29. M. R. Servedio, *Evolution* **54**, 21 (2000).

Acknowledgments: We thank M. Kirkpatrick, S. Otto, M. Whitlock, D. Des Marais, and members of the Rausher and Kirkpatrick laboratory group for advice on this manuscript and S. Scarpino for statistical consultation. We thank the University of Texas Stengl Research Station for field experiment support. This work was supported by NSF grant 0841521 to M.D.R. and a NSF Doctoral Dissertation Improvement Grant to R.H. and M.D.R. R.H. was supported by the NSF Graduate Research Fellowship Program. All data presented here are available in the supporting material.

Supporting Online Material

www.sciencemag.org/cgi/content/full/science.1215198/DC1
Materials and Methods
Figs. S1 and S2
Tables S1 to S9
References

12 October 2011; accepted 12 January 2012
Published online 2 February 2012;
10.1126/science.1215198

Generation of Leaf Shape Through Early Patterns of Growth and Tissue Polarity

Erika E. Kuchen,[1]* Samantha Fox,[1]* Pierre Barbier de Reuille,[2] Richard Kennaway,[2] Sandra Bensmihen,[1] Jerome Avondo,[1] Grant M. Calder,[1] Paul Southam,[2] Sarah Robinson,[1] Andrew Bangham,[2]† Enrico Coen[1]†

A major challenge in biology is to understand how buds comprising a few cells can give rise to complex plant and animal appendages like leaves or limbs. We address this problem through a combination of time-lapse imaging, clonal analysis, and computational modeling. We arrive at a model that shows how leaf shape can arise through feedback between early patterns of oriented growth and tissue deformation. Experimental tests through partial leaf ablation support this model and allow reevaluation of previous experimental studies. Our model allows a range of observed leaf shapes to be generated and predicts observed clone patterns in different species. Thus, our experimentally validated model may underlie the development and evolution of diverse organ shapes.

The shapes of many plant and animal appendages are thought to develop under the influence of orthogonal organizing systems (i.e., systems with axes that intersect at right angles) (*1*–*4*). However, it is unclear how these orthogonal systems lead to changes in tissue shape and how shape changes may themselves feed back to deform the organizing systems. Consider a square piece of tissue that deforms during growth (Fig. 1A). The tissue has an initial linear orthogonal system that organizes the pattern of morphogenesis (Fig. 1B, arrows). We might en-

[1]John Innes Centre, Norwich Research Park, Norwich, NR4 7UH, UK. [2]School of Computing Sciences, University of East Anglia, Norwich Research Park, Norwich, NR4 7TJ, UK.

*These authors contributed equally to this work.
†To whom correspondence should be addressed. E-mail: enrico.coen@jic.ac.uk (E.C.); a.bangham@uea.ac.uk (A.B.)

visage two extreme possibilities as the tissue deforms. One is that the organizing system retains its original arrangement despite the change in tissue shape (Fig. 1C). Another possibility is that the change in shape of the tissue feeds back to deform the organizing system during growth (Fig. 1D).

Here, we exploit live imaging of fluorescently marked *Arabidopsis* leaves to distinguish these possibilities. We concentrated on growth of leaf 1, from when the leaf primordium had a simple dome shape [3 days after initiation (DAI)] to the stage at which the characteristic leaf shape was evident (9 DAI) (fig. S1). We first determined areal growth rates for different regions of the leaf by tracking cell vertices over time. Areal growth rate is lower toward the distal tip of the leaf (Fig. 1J), consistent with previous tracking studies at later stages of growth (*5*–*7*). Areal growth rates also tend to be higher in lateral compared to medial domains (Fig. 1J).

To understand how the observed patterns of growth could be generated, we first considered growth rates in the proximodistal direction along the midline of the leaf lamina (Fig. 1, E to I). At early stages, growth rates parallel to the midline show an almost linear decrease from proximal to distal regions (Fig. 1, E and F). At later stages, the proximodistal gradient in growth rates becomes shallower throughout most of the leaf but maintains a steep decline near the tip (Fig. 1, G to I). To account for these observations, we used a one-dimensional (1D) model with a factor, PGRAD, that declines from proximal to distal positions with an initial linear gradient (fig. S2, A and B) and promotes specified growth rate K (Fig. 1P). PGRAD levels are maintained locally and deform with the tissue during growth. The output of this model is a gradient in growth rates that becomes shallower proximally because these regions extend more rapidly (Fig. 1, E to G, black lines; Fig. 1, H and I, gray lines). Thus, the initial linear gradient is transformed into a curve that dips more steeply toward the distal end.

Although this model generates curves that match the data at early stages (Fig. 1, E to G), observed growth rates at later stages are lower than those predicted by the model (Fig. 1, H and I, gray lines). We therefore introduced a uniformly distributed factor into the model, LATE, that increases during later stages and inhibits the specified growth rates (Fig. 1P and fig. S2C). With this modification, the resulting proximodistal growth rates show a better match to the data (Fig. 1, H and I, black lines).

We next extended the model to 2D, using the growing polarized tissue framework (*8*), in which growth rates can be specified by a distribution of factors over a tissue. Regions of the tissue are mechanically connected, forming a canvas, allowing the deformation resulting from specified local growth patterns to be computed.

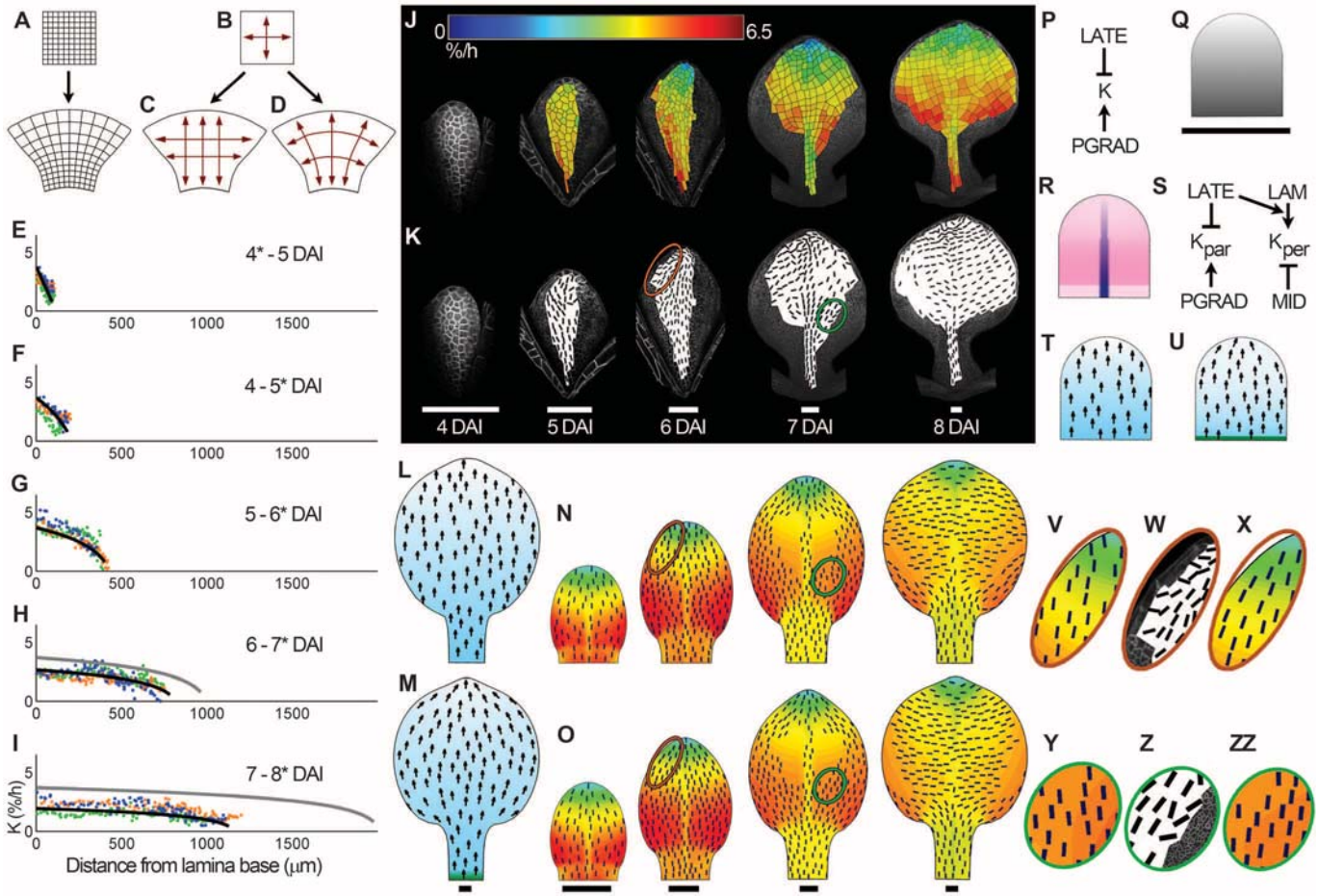

Fig. 1. Leaf growth analysis. (**A**) Tissue deforms through growth. (**B**) Orthogonal organizing system which (**C**) retains its original arrangement or (**D**) deforms during growth. (**E** to **I**) Midline proximodistal growth rates for three replicates (orange, green, and blue), and 1D models (black and gray lines). Distances from lamina base correspond to those on the day indicated by an asterisk. (**J**) Areal growth rates (heat map) and (**K**) principal directions of growth (black lines, where anisotropy > 10%) at the end of each period. (**L**) Resultant shape, POL levels and specified growth orientations (arrows) for nondeforming and (**M**) deforming (organizer-based) models. (**N**) Resultant shapes, areal growth rates, and directions of growth (black lines, where anisotropy > 5%) for 2D nondeforming and (**O**) deforming (organizer-based) models. Heat map and staging as in (J). (**P**) 1D model regulatory network. (**Q**) 2D distribution of PGRAD (gray). (**R**) MID (blue) and LAM (magenta) distributions. (**S**) 2D model regulatory network. (**T**) Initial POL (cyan) distribution for nondeforming and (**U**) deforming models. PROXORG in green. (**V** to **X**) Enlargement of brown ellipses in (N) (K), and (O), respectively. (**Y**, **Z**, and **ZZ**) Enlargement of green ellipses in (N), (K), and (O), respectively. Scale bars, 100 μm.

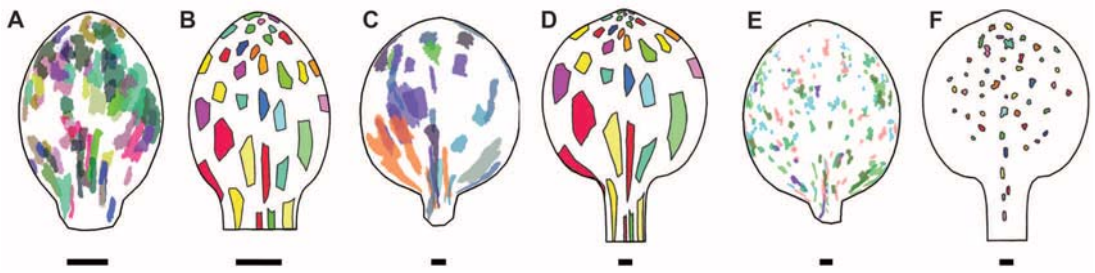

Fig. 2. Clonal analysis. (**A**, **C**, and **E**) Clones induced at 3 DAI (A and C) or 6 DAI (E) and imaged at 6 DAI (A) or 9 DAI (C and E). Clones from several leaves are superimposed. (**B**, **D**, and **F**) Clonal patterns generated by the organizer-based model at stages corresponding to those shown on their left. Scale bars, 100 μm.

Each model has three components: (i) an initial canvas shape with distributed factors; (ii) a system for specifying polarity; and (iii) a growth regulatory network. The starting shape for the canvas is based on a simplified leaf primordium shape (Fig. 1Q and fig. S3). To account for the observed pattern of growth rates (Fig. 1J), the initial canvas has spatial domains defined by three factors: (i) PGRAD is expressed as a linear gradient along the proximodistal axis (as for the 1D model); (ii) LAM is expressed everywhere but at a lower level in a narrow region at the base (which will form the petiole); and (iii) MID is expressed along the midline (Fig. 1, Q and R). For all these factors, levels are maintained locally and deform with the canvas during growth.

Growth orientations depend on a proximodistal gradient of a factor, POLARISER (POL), distributed throughout the canvas (Fig. 1T, arrows). The gradient of POL provides the axiality information needed to specify local growth orientations. We first assumed that growth orientations are specified according to a nondeforming system (Fig. 1C) with axes parallel (proximodistal axis) or perpendicular (mediolateral axis) to the midline (*9*, *10*). This corresponds to keeping the POL gradient parallel to the midline throughout growth (Fig. 1L). There is thus no feedback between tissue deformation and specification of growth orientations. The growth regulatory network controls two specified growth rates: parallel (K_{par}) and perpendicular (K_{per}) to the POL gradient (fig. 1S). K_{par} is controlled by PGRAD and LATE as for the 1D model (Fig. 1P). To account for the higher areal growth rates in the lateral domains, K_{per} is promoted by LAM and inhibited by MID. The extent to which LAM promotes K_{per} is further enhanced by LATE; otherwise, growth rates in the lamina drop below observed levels.

Running this nondeforming model leads to canvas shape changes and patterns of areal growth that are broadly similar to those observed experimentally (Fig. 1N). The principal orientations of resultant growth (Fig. 1N, black lines) switch from being mainly parallel to the midline at early stages to being mainly perpendicular to the midline in the lamina. The switch occurs because LATE enhances the effect of LAM on K_{per} (Fig. 1S).

The principal orientatins of growth predicted by the nondeforming model of leaf development were compared with observed orientations,

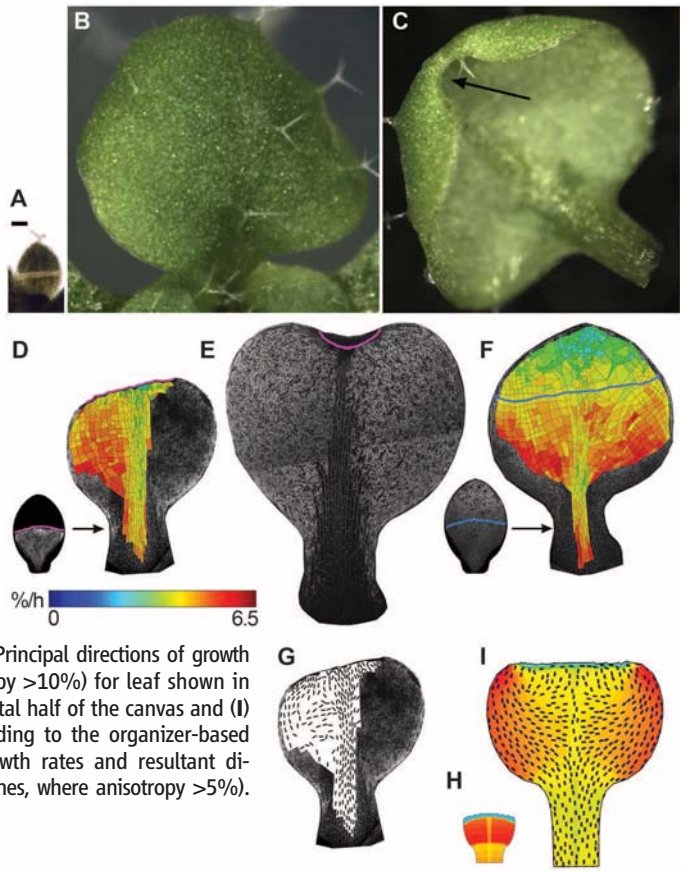

Fig. 3. Distal leaf excision. (**A**) Excision of the distal half of leaf 1 lamina at 6 DAI. Distal region was removed after laser cut (pale line). (**B**) Leaf 1, 6 days after distal excision, viewed from the top and (**C**) from lower (abaxial) side, showing a curved indentation at the tip (arrow). (**D**) Leaf 1 cut at 6 DAI (left) and tracked until 9 DAI (right). Areal growth rates (heat map) calculated over the last 24 hours of tracking. Boundary of cut highlighted with magenta line. (**E**) Leaf after tracking growth for 5 days after distal excision. (**F**) Tracked uncut leaf with a blue line shown at a similar position to the cut in (D). (**G**) Principal directions of growth (black lines, where anisotropy >10%) for leaf shown in (D). (**H**) Excision of the distal half of the canvas and (**I**) output after growth according to the organizer-based model, showing areal growth rates and resultant directions of growth (black lines, where anisotropy >5%). Scale bar, 100 μm.

obtained from the measured displacement of cell vertices (*11*). The observed principal directions of growth are mainly oriented proximodistally at early stages and switch in the lamina toward a more mediolateral orientation during later stages of growth (Fig. 1K), consistent with the nondeforming model (Fig. 1N). However, observed orientations converge toward the leaf tip at early stages much more than those of the model (brown ellipses, Fig. 1, K, N, V, and W, and fig. S4, A and B). Also, in the proximal lamina regions near the midvein, principal orientations of growth are oblique and diverge from the midline at later stages (green ellipses, Fig. 1, K and Z and fig. S4, C and D), in contrast to the largely parallel or perpendicular orientations predicted by the model (green ellipse, Fig. 1, N and Y).

We next considered an organizer-based model in which POL distribution arises by propagation through the canvas and then deforms during growth. POL production is promoted at the base of the canvas through an identity factor PROXORG (proximal organizer) and is degraded everywhere at a constant rate (Fig. 1U). Propagation of POL through the canvas generates a proximodistal field of polarities that is initially parallel to the midline in the basal half of the canvas and converges toward the tip (Fig. 1U and fig. S5A) but then deforms (Fig. 1M and fig. S5B). The initial canvas, distribution of factors, and growth regulatory network are the same as in the nondeforming model (Fig. 1, Q to S). The resulting shape changes and growth patterns are also similar (Fig. 1O and fig. S5C). However, resultant growth orientations give a better match to the experimental data (table S1): Orientations converge toward the leaf tip (brown ellipse, Fig. 1, O and X) and have oblique orientations of growth that diverge from the midline at later

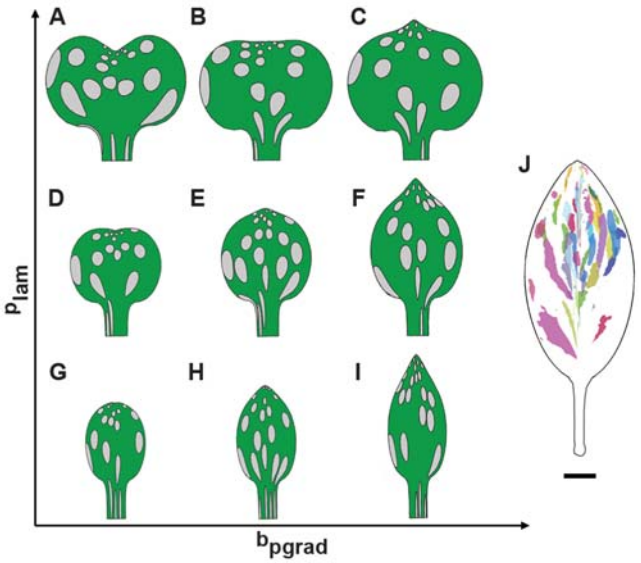

Fig. 4. Generation of diverse leaf shapes. (**A** to **I**) Morphospace generated from the organizer-based model, varying two growth parameters; the strength of promotion by LAM, p_{lam}, and the level of PGRAD at the distal end b_{pgrad}. *Arabidopsis* leaf 1 corresponds to (E). Clones induced as circles on day 3. (**J**) Clones on mature leaf (metamer 4) of *Antirrhinum*, induced when the leaf primordium is about 50 to 100 μm wide. Clones on the petiole were not recorded. Scale bar for *Antirrhinum* leaf, 1 cm.

stages due to deformation of the canvas (green ellipse, Fig. 1, O and ZZ).

An organizer-based model is also consistent with patterns of polarity observed in young leaf primordia. PIN1 (PIN-FORMED1) auxin transporters at this stage are oriented in a proximodistal pattern, with cell polarity pointing distally and converging toward the tip in the epidermis or pointing proximally in internal tissues (*12*). Both polarity patterns are consistent with an organizer-based model, because specifying growth orientation depends only on the axiality component of the polarity field, not the sense in which the polarity points (*8*). The mechanism determining PIN polarity is still unclear (*13*). One possibility is that auxin plays a primary role in establishing this pattern and would therefore be influenced by organizers of polarity. Alternatively, the PIN polarity pattern may be a read-out of a separate underlying polarity system.

The organizer-based model should account for growth patterns across the entire leaf as well as in regions accessible to tracking. This additional requirement was evaluated through clonal analysis. Clones were induced at 3 DAI (Fig. 2, A and C) or 6 DAI (Fig. 2E) using a heat shock–inducible Cre-Lox system (*14*). For regions accessible to tracking, the resulting clones were in good agreement with the fate of individually tracked cells (fig. S6). Clonal patterns were also compared with those generated by the organizer-based model. This was achieved by superimposing outlines of leaf cells on the canvas (fig. S3) and then growing the canvas to its final shape (Fig. 2, B, D, and F). The shapes and orientations of predicted and observed clones showed a good qualitative match: Clones diverge near the lamina base and converge toward the tip.

A key assumption of the above models is that the spatial pattern of growth rates is established at an early stage of leaf development. This assumption does not rule out modulations in growth pattern at later stages but seems inconsistent with the claim that leaves regenerate after excision of the distal half at a time after patterning has been established according to our models (*15*). To investigate this discrepancy, we repeated the excision experiment by removing the distal half of the leaf at a similar developmental stage to that previously reported to give regeneration (6 DAI) (Fig. 3A and fig. S7A) (*15*). As with the previously published experiments, the cut edge was clearly evident after 2 days of growth but seemed to have disappeared after a further 4 days of growth when the leaf was viewed from above (Fig. 3B). However, examination of the underside of the leaf revealed a semicircular edge at the tip similar in length to the original cut, suggesting that regeneration from the cut edge may not have occurred (Fig. 3C). Tracking leaf development after distal excision revealed a similar spatial pattern of growth rates to a control uncut leaf, except for regions near the cut, where growth rates were reduced (Fig. 3, D and F). There was no evidence of tip regeneration (Fig. 3, D and E). The superficial resemblance to regeneration (Fig. 3B) is a consequence of the high contribution that proximal regions of the leaf primordium make to the mature leaf, and the reduced growth rate of the cut edge.

To determine whether the organizer-based model could account for the observed effects of distal excision, we grew the canvas until day 6 and then removed the distal half (Fig. 3H and fig. S2, D and E). Growth is assumed to be unaffected except at the cut margin, where growth is inhibited. The final shape and growth patterns generated by the model are broadly similar to that observed experimentally after distal excision (Fig. 3, G and I). Thus, distal excision validates the model rather than refuting it.

To determine whether the organizer-based model could account for leaf shapes other than leaf 1 in *Arabidopsis*, we varied each of the model's growth parameters (fig. S8). The effect of varying b_{pgrad} (the level of PGRAD at the distal end) and p_{lam} (the strength of K_{per} promotion by LAM) in various combinations is shown in Fig. 4. The resulting morphospace includes many botanically described leaf shapes, such as obcordate (Fig. 4, A and D), ovate (Fig. 4F), and elliptic (Fig. 4, H and I) (*16*). Thus, the model may underlie a wide range of leaf forms.

As a further test of the model's generality, we compared the pattern of clones predicted to those observed in *Antirrhinum*, a species with an elliptic leaf shape amenable to clonal analysis (*9*). Clones were induced at an early stage of leaf development in *Antirrhinum*, using a temperature-sensitive transposon, and visualized in the mature leaf. The pattern of clones observed is in broad agreement with those generated by the model with low p_{lam}: Large narrow clones diverge outward from the lamina base, and small clones converge toward the tip (Fig. 4, H and J).

These results show that a relatively simple model can broadly account for the growth dynamics and shape changes observed during normal and perturbed growth of *Arabidopsis* and may also underlie a variety of other leaf shapes. The model assumes that growth orientations are specified through a tissue polarity system that deforms during growth and that a basic pattern of growth rates across the leaf is established from an early stage. This raises the question of how these features are specified at the cellular scale and what genes may underlie them. Candidate genes for LAM are *LEAFY PETIOLE* (*17*) and members of the *YABBY* family (*18*), which are expressed in the lamina and promote its lateral growth. Candidate organizers of tissue polarity are the *CUP-SHAPED COTYLEDON* (*CUC*) genes, which are expressed at the base of the leaf (*19*) and play a key role in leaf development (*20*, *21*). Thus, our model provides a simple unifying framework for the control of organ shape that can be further tested experimentally, elaborated through the incorporation of genes and cellular properties, and extended to cover more complex leaf shapes.

References and Notes

1. L. I. Held, *Imaginal Discs: The Genetic and Cellular Logic of Pattern Formation* (Cambridge Univ. Press, Cambridge, 2002).
2. G. T. Kim, K. H. Cho, *Physiol. Plant.* **126**, 494 (2006).
3. G. F. Stopper, G. P. Wagner, *Dev. Biol.* **288**, 21 (2005).
4. L. Wolpert, C. Tickle, *Principles of Development* (Oxford Univ. Press, Oxford, ed. 4, 2011).
5. G. S. Avery, *Am. J. Bot.* **20**, 565 (1933).
6. D. Schmundt, M. Stitt, B. Jahne, U. Schurr, *Plant J.* **16**, 505 (1998).
7. S. D. Wolf, W. K. Silk, R. E. Plant, *Am. J. Bot.* **73**, 832 (1986).
8. R. Kennaway, E. Coen, A. Green, A. Bangham, *PLOS Comput. Biol.* **7**, e1002071 (2011).
9. A.-G. Rolland-Lagan, J. A. Bangham, E. Coen, *Nature* **422**, 161 (2003).
10. A. J. Fleming, *Plant Biol.* **5**, 341 (2003).
11. Z. Hejnowicz, J. A. Romberger, *J. Theor. Biol.* **110**, 93 (1984).

12. E. Scarpella, D. Marcos, J. Friml, T. Berleth, *Genes Dev.* **20**, 1015 (2006).
13. Y. Boutté, Y. Ikeda, M. Grebe, *Curr. Opin. Plant Biol.* **10**, 616 (2007).
14. J. L. Gallois, C. Woodward, G. V. Reddy, R. Sablowski, *Development* **129**, 3207 (2002).
15. G. Sena, X. Wang, H.-Y. Liu, H. Hofhuis, K. D. Birnbaum, *Nature* **457**, 1150 (2009).
16. F. Swink, G. Wilhelm, *Plants of the Chicago Region* (Indiana Academy of Science, Indianapolis, ed. 4, 1994).
17. E. van der Graaff, A. D. Dulk-Ras, P. J. J. Hooykaas, B. Keller, *Development* **127**, 4971 (2000).
18. R. Sarojam *et al.*, *Plant Cell* **22**, 2113 (2010).
19. M. Aida, T. Ishida, M. Tasaka, *Development* **126**, 1563 (1999).
20. A. Hasson *et al.*, *Plant Cell* **23**, 54 (2011).
21. G. D. Bilsborough *et al.*, *Proc. Natl. Acad. Sci. U.S.A.* **108**, 3424 (2011).

Acknowledgments: This work was funded by the U.K. Biotechnology and Biological Sciences Research Council (BBSRC). We thank S. Sauret-Güeto, C. Hindle, and J. Chan for help in developing the tracking chamber; K. Lee for imaging cut leaves with OPT; and S. Grandison for mathematical support. The authors declare no competing financial interests.

Further information and software can be downloaded at www.uea.ac.uk/cmp/research/cmpbio/Gftbox.

Supporting Online Material
www.sciencemag.org/cgi/content/full/335/6072/1092/DC1
Materials and Methods
SOM Text
Figs. S1 to S8
Table S1
References (*22*–*31*)

30 September 2011; accepted 24 January 2012
10.1126/science.1214678

Elastic Domains Regulate Growth and Organogenesis in the Plant Shoot Apical Meristem

Daniel Kierzkowski,[1]* Naomi Nakayama,[1]* Anne-Lise Routier-Kierzkowska,[1]* Alain Weber,[1]* Emmanuelle Bayer,[2] Martine Schorderet,[3] Didier Reinhardt,[3] Cris Kuhlemeier,[1] Richard S. Smith[1]†

Although genetic control of morphogenesis is well established, elaboration of complex shapes requires changes in the mechanical properties of cells. In plants, the first visible sign of leaf formation is a bulge on the flank of the shoot apical meristem. Bulging results from local relaxation of cell walls, which causes them to yield to internal hydrostatic pressure. By manipulation of tissue tension in combination with quantitative live imaging and finite-element modeling, we found that the slow-growing area at the shoot tip is substantially strain-stiffened compared with surrounding fast-growing tissue. We propose that strain stiffening limits growth, restricts organ bulging, and contributes to the meristem's functional zonation. Thus, mechanical signals are not just passive readouts of gene action but feed back on morphogenesis.

The plant shoot apical meristem is composed of two regions, the slow-growing central region, which contains the stem cell niche, and the surrounding periphery, where cells divide rapidly and new organs are initiated (*1*–*4*). New organ primordia initiate at accumulation points of the plant hormone auxin (*5*–*7*). In addition to triggering gene regulatory pathways, auxin induces cell wall acidification (*8*), which increases expansin activity (*9*) that modifies cross-links in the cell wall matrix. Disruption of auxin signaling suppresses organ initiation, which can be restored by the local application of auxin (*7*, *10*, *11*). Bulging in the meristem flank can also be triggered by local cell wall loosening with expansin (*12*, *13*) or pectin methyl-esterase (PME) (*14*, *15*). These bulges can develop into normal organs, which suggests that a mechanical signal is involved in primordium differentiation. Additional support for mechanical signals in this pathway comes from the recent hypothesis that stress in the cell wall is the signal that orients the microtubule network and the PIN-FORMED 1 (PIN1) auxin transporter (*16*, *17*). Yet despite the accumulating evidence for an instructive role for mechanical signals in organogenesis, the mechanical properties of the shoot apex have only recently begun to be explored (*15*, *18*). Here, we examine both the elastic and plastic properties of the shoot apex and link them to growth dynamics.

Tomato vegetative shoot apices were imaged at 11-hour intervals by confocal microscopy in order to monitor their growth. Images were analyzed with MorphoGraphX (*19*) (Fig. 1) to compute relative changes in cell surface area (Fig. 2). Cell surface expansion was 25% on average in the central region and between 45 and 80% on average in the periphery, depending on the stage of development of the adjacent primordium. The boundary region between the primordium and the meristem displayed little growth. Our data closely resembled growth patterns in other species (*1*–*4*).

In order to examine meristem material properties, we induced tissue deformation by manipulating turgor pressure with osmotic treatments using mannitol and NaCl. Experiments started by adapting the samples in solutions of 0.2 M osmotically active molecules. Subsequent immersion in hypo-osmotic medium (0 M) resulted in a relative increase in total surface area of 6 ± 2% (n = 20). The treatment revealed regional differences, with cells in the central and boundary regions expanding less than those in the periphery (Fig. 3B, fig. S1A, and fig. S2B). Deflation in hyperosmotic solution (0.4 M) resulted in average shrinkage of 6 ± 2% (n = 17). The relative area decrease was high for cells at the apex summit and variable on the flank (Fig. 3C, fig. S1B, and fig. S2C). The effects were independent of the type of osmolyte used. In order to distinguish between elastic and plastic deformations resulting from hypo-osmotic treatments, we performed sequential treatment with 0 M medium followed by a return to 0.2 M. Whereas the hypo-osmotic treatment resulted in a 7 ± 1% (n = 5) total area increase, after returning to 0.2 M solution, the apices were irreversibly expanded by 2 ± 1%. Therefore, the total expansion after an increase in turgor pressure is primarily an elastic response.

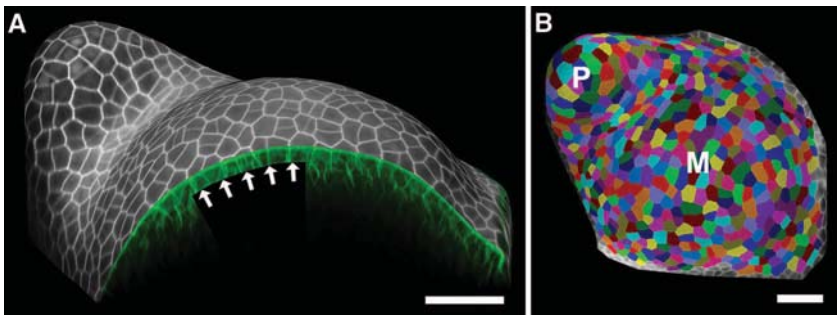

Fig. 1. Quantitative analysis of tissue deformation with MorphoGraphX (www.MorphoGraphX.org). (**A**) Cell wall signal from the epidermal layer was projected onto a curved surface mesh of the apex. (**B**) The surface is then segmented into cells and used to track local tissue deformation. P, youngest primordium; M, meristem, Scale bars, 40 μm.

[1]Institute of Plant Sciences, University of Bern, Altenbergrain 21, CH-3013 Bern, Switzerland. [2]CNRS—Laboratoire de Biogenèse Membranaire, UMR5200, 146 rue Leo Saignat, F-33076 Bordeaux, France. [3]Department of Biology, University of Fribourg, Chemin de Musée 10, CH-1700 Fribourg, Switzerland.

*These authors contributed equally to this work.
†To whom correspondence should be addressed. E-mail: richard.smith@ips.unibe.ch